Oxidative nitration reaction of antiaromatic 5,15-dioxaporphyrin

Nishiyama, Akihide
Department of Chemistry and Biochemistry, Graduate School of Engineering, Kyushu University

Tanaka, Yuki
Department of Chemistry and Biochemistry, Graduate School of Engineering, Kyushu University

Mori, Shigeki
Advanced Research Support Center (ADRES), Ehime University

Furuta, Hiroyuki
Department of Chemistry and Biochemistry, Graduate School of Engineering, Kyushu University

他

出版情報：Journal of Porphyrins and Phthalocyanines. 24 (01n03), pp.355-361, 2020-01-01. World Scientific Publishing
バージョン：
権利関係：

Oxidative nitration reaction of antiaromatic 5,15-dioxaporphyrin

Akihide Nishiyama[a], Yuki Tanaka[a], Shigeki Mori[b], Hiroyuki Furuta*[ac◊], Soji Shimizu*[ac◊]

[a] *Department of Chemistry and Biochemistry, Graduate School of Engineering, Kyushu University, Fukuoka 819-0395, Japan*

[b] *Advanced Research Support Center (ADRES), Ehime University, Matsuyama 790-8577, Japan*

[c] *Center for Molecular Systems (CMS), Kyushu University, Fukuoka 819-0395, Japan*

Dedicated to Professor Atsuhiro Osuka on the occasion of his 65th birthday

Received date (to be automatically inserted after your manuscript is submitted)
Accepted date (to be automatically inserted after your manuscript is accepted)

ABSTRACT: Upon oxidation of 20π-electron antiaromatic 5,15-dioxaporphyrin (DOP) using nitrosonium ions as oxidants, a tetrakis-β-nitrated compound was formed instead of the expected 18π-electron aromatic dication species via an oxidative nitration reaction mechanism. Compared with the original DOP, this tetranitro DOP product exhibited a blue-shift of absorption and down-field shifts of the β-pyrrolic proton signals. The unique antiaromatic electronic structure of the tetranitro DOP was experimentally disclosed by electrochemistry and theoretically by DFT and NICS calculations.

KEYWORDS: 5,15-dioxaporphyrin, antiaromaticity, oxidative nitration

◊ SPP full member in good standing

*Correspondence to: Hiroyuki Furuta, email: hfuruta@cstf.kyushu-u.ac.jp and Soji Shimizu, email: ssoji@cstf.kyushu-u.ac.jp, fax: +81 92-802-2866

INTRODUCTION

Heteroatom-containing porphyrin analogues form an important class of porphyrinoid [1, 2] from the early stage of the porphyrin chemistry because unique properties of porphyrin such as UV/vis absorption, redox, and metal coordination properties can be diversified by the introduction of heteroatoms into the porphyrin skeleton [3]. Among heteroatom-containing porphyrinoids, replacement of carbon atoms at the *meso*-positions with heteroatoms can cause drastic changes of properties as represented by phthalocyanine as an azaporphyrinoid [4], which exhibits totally different blue or green color compared to the red color of regular porphyrins [5]. In addition to the artificially-made phthalocyanine for industrial applications, such *meso*-heteroatom-containing porphyrinoids play important roles in biological processes. For example, during the heme catabolism, verdoheme, an iron complex of *meso*-monooxaporphyrin, is initially formed and further oxidized into an open-chain biliverdin [6, 7].

Recently, our group revealed that the replacement of one more *meso*-carbon atom with an oxygen atom to form 5,15-dioxaporphyrin (DOP, **1**) can convert the 18π-electron aromatic conjugated system of porphyrin into a stable 20π-electron antiaromatic conjugated system due to the insertion of lone-pair electrons of the oxygen atoms into the porphyrinic π-system (Fig. 1) [8]. Heteroatom-substitution toward the creation of stable antiaromatic porphyrinoids has also been proved to be effective independently by Matano and Shinokubo with 5,15-diaminoporphyrins bearing saturated amino-nitrogen atoms at the face-to-face *meso*-positions [9–12]. Recently, Matano and our group reported that 15-amino-5-oxaporphyrin can also attain 20π antiaromaticity [13]. Furthermore, Matano *et al.* disclosed interconversion between antiaromatic 20π neutral species, 19π radical cation, and aromatic 18π dication by stepwise oxidation and reduction. In contrast to the facile interconversion of 5,15-diaminoporphyrin and 15-amino-5-oxaporphyrin to the aromatic dication species, a β,β-linked dimer was formed upon oxidation of DOP with $AgPF_6$ (Fig. 1) [8]. This unique reactivity was ascribed to the large spin density distribution and less steric hindrance around the β-pyrrolic positions adjacent to the *meso*-oxygen atoms. During our attempts to obtain an 18π dication species of DOP using various oxidants, we noticed that the oxidation of DOP using nitrosonium hexafluoroantimonate ($NOSbF_6$) as an oxidant provided a different product, which was characterized as tetrakis-β-nitrated DOP (tetranitro DOP, **2**) by high-resolution mass spectrometry and single crystal X-ray diffraction analysis. This rather unexpected nitration proceeded via oxidative nitration reaction mechanism, which was proposed for electron-rich arene molecules by Kochi *et al*. [14] We report herein the the synthesis and optical and electrochemical properties of this unique tetranitro DOP.

EXPERIMENTAL

General procedure

Electronic absorption spectra were recorded on a JASCO V-770. Magnetic circular dichroism (MCD) spectra were recorded on a JASCO J-1500 spectrodichrometer by applying parallel and antiparallel magnetic fields to the light propagation with a 1.6 T permanent magnet (T = tesla). ^{1}H NMR spectra were recorded on a JEOL ECX-500 spectrometers (operating at 495.13 MHz for ^{1}H) using residual solvent as an internal reference for ^{1}H (δ_H = 7.26 ppm for $CDCl_3$). High resolution mass spectrometry was performed on a JEOL LMS-HX-110 spectrometer (FAB mode with 3-nitrobenzyl alcohol (NBA) as a matrix). Thin-layer chromatography (TLC) was carried out on aluminum sheets coated with silica gel 60 F_{254} (MERCK). Dry acetonitrile and CH_2Cl_2 were purchased from KANTO CHEMICAL. All other reagents and solvents were of commercial reagent grade and were used without further purification except where noted.

Crystallographic data collection and structure refinement

Suitable crystals of **2** for X-ray diffraction analysis were obtained from the vapor diffusion of methanol into a THF solution of **2**. Data collection was carried out at –173 °C on a Rigaku Saturn724 diffractometer with MoKα radiation. The structure was solved by a direct method (SHELXT) [15, 16] and refined using a full-matrix least squares technique (SHELXL) [17]. CCDC-1934519 contains the supplementary crystallographic data for this paper. These data can be obtained free of charge from the Cambridge Crystallographic Data Centre via www.ccdc.cam.ac.uk/structures.

Cyclic voltammetry

A cyclic voltammogram was recorded on a CH Instrument Model 620B (ALS) under an argon atmosphere in a CH_2Cl_2 solution with 0.1 M tetra-*n*-butylammonium hexafluorophosphate as a supporting electrolyte. Measurements were made with a glassy carbon working electrode, an Ag/AgCl reference electrode, and a Pt wire counter electrode. The concentration of the solution was fixed at 0.5 mM, and the sweep rate was set to 100 mV s^{-1}. The ferrocenium/ferrocene (Fc^+/Fc) couple was used as an internal standard.

DFT, TDDFT, and NICS calculations

Gaussian 16 [18] software package was used to carry out the density functional theory (DFT) and time-dependent DFT (TDDFT) calculations using a B3LYP functional with a 6-31G(d) basis set, and Nucleus-Independent Chemical Shift (NICS) calculations using a B3LYP functional with a SDD basis set for a nickel and a 6-311G(2d,p) basis set for the rest. The anisotropy of the current-induced density (ACID) calculations were performed by employing the continuous set of gauge transformations (CSGT) method to calculate the current densities at the level of B3LYP/SDD for a nickel and 6-311G(2d,p) for the rest, and the results were plotted using POV-Ray 3.7 beta for Windows.

Synthesis

1 (42 mg, 69 μmol) in dry CH_2Cl_2 (8 mL) was stirred at room temperature under N_2 atmosphere. Then an acetonitrile solution (8 mL) of $NOSbF_6$ (40 mg, 0.15 mmol, 2.2 eq) was added. The resultant mixture was stirred for 10 min. After removal of the solvent under vacuum by a rotary evaporator, the residue was reprecipitated from $CHCl_3$ and diethyl ether to provide **2** as a dark green solid in 23% yield (13 mg, 16 μmol).
HRMS (FAB): *m*/*z* 788.1121 (calcd for $C_{36}H_{26}N_8O_{10}Ni$, [M^+] 788.1125); ^{1}H NMR (495 MHz, $CDCl_3$, 297 K): δ_H, ppm 6.96 (s, 4H, β-pyrrole), 6.85 (s, 4H, mesityl), 2.36 (s, 6H, mesityl), 2.12 (s, 12H, mesityl). UV/vis/NIR ($CHCl_3$): λ_{max}, nm (ε) 511 (64600), 436 (18800), 309 (7240).

RESULTS AND DISCUSSION

Tetranitro DOP **2** was obtained in 23% yield by oxidation of DOP **1** with nitrosonium hexafluoroantimonate ($NOSbPF_6$) in dry dichloromethane (Scheme 1). Recrystallization of the reaction mixture provided pure **2** as a dark green solid. **2** was characterized by high-resolution mass spectrometry and single crystal X-ray diffraction analysis (Fig. 2) [19]. The crystal structure of **2** was determined as its axially methoxy adduct because crystals were grown from THF and methanol. The nitro groups were substituted at the four β-positions adjacent to the *meso*-oxygen atoms. **2** possesses a planar structure with small root-mean-square deviation (d_{RMS}) of 0.065 Å, which is similar to that of **1** with pyridine ligands at the axial positions (d_{RMS} = 0.033). The nitro groups were only slightly tilted from the mean plane of the DOP core by 3–7°. Apparent bond length alternation can be seen for the C–C bonds of the pyrrole rings (C1–C2: 1.426(3) Å, C2–C3: 1.374(3) Å, C3–C4: 1.408(2) Å, C6–C7: 1.412(3) Å, C7–C8: 1.373(3) Å, and C8–C9: 1.431(3) Å), whereas

there is almost no bond length alternation in the pyrrole-bridging C–O bonds (C1–O1: 1.358(2) Å and C9–O2: 1.355(2) Å) and C–C bonds (C4–C5: 1.403(3) Å and C5–C6: 1.399(3) Å). This is indicative of effective π-conjugation of the *meso*-oxygen atoms. The overall bond length alternation was quantified by the harmonic oscillator model of aromaticity (HOMA) [20] value, which becomes close to 1 for aromatic molecules. Although the correlation between the antiaromaticity and the HOMA values has not yet been clarified, the HOMA values of **1** and **2** (**1**: 0.72 [8], **2**: 0.68) are relatively high.

Despite the red-shift, the UV/vis/NIR absorption spectrum of **2** was broadly similar to that of **1** [8], exhibiting intense bands at 511 and 436 nm with a shoulder at 480 nm and broad, structureless band in the NIR region (Fig. 3). Corresponding to these intense bands, negative-to-positive Faraday *B* terms at 511 and 438 nm were observed in the magnetic circular dichroism (MCD) spectrum. The observed absorption bands can be assigned based on Michl's perimeter model for 4N-electron annulene systems, in which six frontier orbitals (*h*–, *h*+, *s*–, *s*+, *l*–, and *l*+) derived from a symmetry perturbation of the degenerate HOMO, singly-occupied molecular orbital (SOMO), and LUMO of the 4N-electron perimeter are involved [21–23]. Corresponding molecular orbitals (MOs) were shown in Fig. 4. Compared with **1**, these MOs were significantly stabilized due to the electron-withdrawing nitro groups.

According to Michl's perimeter model, the main transitions of antiaromatic compounds consist of a weak S band, less intense N bands, and intense P bands, which arise from transitions between the six frontier MOs. The S band mainly comprising transitions between *s*– and *s*+ orbitals is forbidden because of its intrashell transition nature. In contrast, pairs of the N and P bands (N_1 and P_1 and N_2 and P_2) arise from the configurational interactions between *s*– → *l*– and *h*+ → *s*+ transitions and between *s*– → *l*+ and *h*– → *s*+ transitions, respectively. The main bands at 511 and 436 nm can be assigned as P_1 and P_2 bands, whereas the broad NIR absorption with forbidden nature is ascribed to the S band. The time-dependent (TD)DFT calculation supported this band assignment (Table 1). The overall absorption spectral profile of **2**, therefore, reflects its antiaromatic electronic structure.

In the ^{1}H NMR spectrum of **2**, β-pyrrolic protons were resonated at δ_H = 6.96 ppm, which is significantly down-field shifted compared with those of **1** at δ_H = 5.66 and 5.12 ppm. To obtain in-depth insight into the paratropic ring current effect, the nucleous-independent chemical shift (NICS) values were calculated at positions designated in Fig. 5 [24]. Despite the positive NICS(1) values of δ = 4.0 and 3.5 ppm estimated at the 2,4,6,8-positions, the smaller NICS(1) values compared with those of **1** (δ = 7.7 and 6.7 ppm) have a good correlation with the observed down-field shifts of the β-pyrrolic protion signals of **2**. Meanwhile, the lager negative NICS(1) values of δ = –5.3 ppm inside the pyrrole rings than those of **1** (δ = –4.3 ppm) implied greater contribution of aromatic local ring current effects of the pyrrole rings than the global antiaromatic ring current. Although further quantitative discussion is necessary, the anisotropy of the current-induced density (ACID) plots of **1** and **2** imply attenuated antiaromaticity of **2** from that of **1** (Fig. 6) [25, 26].

In addition, introduction of the nitro groups gave an impact on the redox potentials (Fig. 7). In the cyclic voltammogram, **2** exhibited pseudoreversible oxidation waves at 1.02 and 1.14 V vs. Fc^+/Fc and reduction waves at –0.89 and –1.09 V, which were significantly shifted to the positive potential direction from those of **1** (oxidation potentials: 0.05 and 0.68 V and reduction potentials: –1.34 and –1.87 V) [8]. For all of the redox waves, the currents in the backward scan were smaller than those in the forward scan. These electrochemical results indicate that the electron-withdrawing nitro groups stabilize the HOMO and LUMO energy levels, but electrochemically-generated species are rather unstable. The MO diagrams also supported the significant stabilization of the frontier molecular orbitals derived from the 20π-antiaromatic conjugated system of DOP (Fig. 4).

Tetranitration reaction of **2** is thought to proceed via an oxidative nitration mechanism proposed for nitration of arenes with nitrosonium ions by Kochi *et al*. [14] In the first step, oxidation of DOP by a nitrosonium ion (NO^+)

produces a radical cation of DOP and nitric oxide (NO). The produced NO is prone to be oxidized to NO_2 in the presence of air. Subsequent coupling of the radical cation of DOP and NO_2 leads to nitration of DOP. Since the spin density of radical cation is localized on the β-positions adjacent to the *meso*-oxygen atoms according to our previous study [8], nitration selectively occurs on these β-positions. Despite the putative shifts of oxidation potentials to the positive potential direction by nitration, only the tetranitrated product (**2**) was obtained. This can be explained in terms of oxidation property of the nitrosonium ion, which is strong enough to oxidize partially nitrated DOP intermediates, and increasing stability upon increment of the number of electron-withdrawing nitro groups.

CONCLUSION

In summary, tetranitro DOP **2** was unexpectedly obtained though the oxidative nitration reaction with nitrosonium ion. This reaction mechanism was initially proposed for aromatic arene, but was observed for the first time for antiaromatic compounds. Because of the inherently unstable electron configuration of antiaromatic compounds, the nitration reaction is reasonably accelerated to provide the stable tetranitrated product. Despitet the down-field shift of the β-pyrrolic proton signal and the small positive NICS(1) values, **2** retains a certain antiaromaticity, judging from the similar UV/vis/NIR absorption spectral profile to that of **1**, which can be characterized as a 4N-electron antiaromatic system according to Michl's terminology.

Despite the expectation of antiaromatic compounds as functional materials in modern organic electronics, there has been less knowledge about the properties and reactivities of antiaromatic compounds compared to aromatic compounds. As evidenced by this work, heteroatom-introduction to the π-conjugated system of porphyrin is a highly potential method to create stable antiaromatic compounds. Piling up of the knowledge of reactivities using DOP as a stable antiaromatic platform and further synthetic investigation of other types of heteroatom-containing porphyrinoids will open a new stage for antiaromatic compounds as functional materials. Investigation along these lines is intensively being pursuit in our laboratory.

Acknowledgements

This work was supported by Grants-in-Aids for Young Scientists A and (JSPS KAKENHI Grant Number JP26708003), Scientific Research (B) (JSPS KAKENHI Grant Number JP19H02703), and Scientific Research on Innovative Area, "π-System Figuration: Control of Electron and Structural Dynamism for Innovative Functions (No. 2601)" (JSPS KAKENHI Grant Number JP17H05160).

REFERENCES

1. Sessler JL and Weghorn SJ. *Expanded, Contracted, and Isomeric Porphyrins*; Pergamon Press: New York, 1997
2. Sessler JL, Gross Z and Furuta H. *Chem. Rev.* 2017; **117**: 2201–2202.
3. Reddy BK, Basavarajappa A, Ambhore MD and Anand VG. *Chem. Rev.* 2017; **117**: 3420−3443.
4. *Phthalocyanine: Properties and Applications*, Leznoff CC and Lever ABP. (Eds.) Wiley-VCH: New York, 1989-1996; Vol. 1–4
5. Matano Y. *Chem. Rev.* 2017; **117**: 3138–3191.
6. Sato H, Higashimoto Y, Sakamoto H, Sugishima M, Takahashi K, Palmer G and Noguchi M. *J. Inorg. Biochem.* 2007; **101**: 1394–1399.
7. Sato H, Higashimoto Y, Sakamoto H, Sugishima M, Shimokawa C, Harada J, Palmer G and Noguchi M. *J. Inorg. Biochem.* 2011; **105**: 289–296.
8. Nishiyama A, Fukuda M, Mori S, Furukawa K, Fliegl H, Furuta H and Shimizu S. *Angew. Chem. Int. Ed.* 2018; **57**: 9728–9733.
9. Satoh T, Minoura M, Nakano H, Furukawa K and Matano Y. *Angew. Chem. Int. Ed.* 2016; **55**: 2235–2238.

10. Sudoh K, Satoh T, Amaya T, Furukawa K, Minoura M, Nakano H and Matano Y. *Chem. Eur. J.* 2017; **23**: 16364–16373.
11. Sudoh K, Hatakeyama T, Furukawa K, Nakano H and Matano Y. *J. Porphyrins Phthalocyanines* 2018; **22**: 542–551.
12. Yamaji A, Tsurugi H, Miyake Y, Mashima K and Shinokubo H. *Chem. Eur. J.* 2016; **22**: 3956–3961.
13. Sudoh K, Furukawa K, Nakano H, Shimizu S and Matano Y. *Heteroatom Chem.* 2018; **8**: e21456.
14. Kim EK and Kochi JK. *J. Org. Chem.* 1989; **54**: 1692–1702.
15. Sheldrick G. *Acta Crystallogra., Sect. A: Found. Crystallogra.* 2008; **64**: 112–122.
16. Sheldrick G. *Acta Crystallogra., Sect. A: Found. Crystallogra.* 2015; **71**: 3–8.
17. Sheldrick G. *Acta Crystallogr., Sect. C: Cryst. Sctruct. Commun.* 2015; **71**: 3-8.
18. Gaussian 16, Revision A.03, Frisch MJ, Trucks GW, Schlegel HB, Scuseria GE, Robb MA, Cheeseman JR, Scalmani G, Barone V, Petersson GA, Nakatsuji H, Li X, Caricato M, Marenich AV, Bloino J, Janesko BG, Gomperts R, Mennucci B, Hratchian HP, Ortiz JV, Izmaylov AF, Sonnenberg JL, Williams-Young D, Ding F, Lipparini F, Egidi F, Goings J, Peng B, Petrone A, Henderson T, Ranasinghe D, Zakrzewski VG, Gao J, Rega N, Zheng G, Liang W, Hada M, Ehara M, Toyota K, Fukuda R, Hasegawa J, Ishida M, Nakajima T, Honda Y, Kitao O, Nakai H, Vreven T, Throssell K, Montgomery J, J. A., Peralta JE, Ogliaro F, Bearpark MJ, Heyd JJ, Brothers EN, Kudin KN, Staroverov VN, Keith TA, Kobayashi R, Normand J, Raghavachari K, Rendell AP, Burant JC, Iyengar SS, Tomasi J, Cossi M, Millam JM, Klene M, Adamo C, Cammi R, Ochterski JW, Martin RL, Morokuma K, Farkas O, Foresman JB, and Fox DJ; Gaussian, Inc.: Wallingford CT, 2016.
19. Crystallographic data for **2**. $C_{38}H_{34}N_8NiO_{12}$, Mw = 853.43, monoclinic, space group $P2_1/c$ (No. 14), a = 9.5492(3), b = 14.7886(5), c = 13.1978(4) Å, β = 92.850(3)°, V = 1861.48(10) Å^3, Z = 2, T = –173 °C, 31530 measured reflections, 4490 unique reflections (R_{int} = 0.0584), R = 0.0400 ($I > 2$ s(I)), R_w = 0.0891 (all data), goodness-of-fit on F_2 = 1.032, largest diff. peak/hole 0.36 and –0.38 e Å^{-3}.
20. Krygowski TM, Szatylowicz H, Stasyuk OA, Dominikowska J and Palusiak M. *Chem. Rev.* 2014; **114**: 6383–6422.
21. Howeler U, W. Downing J, Fleischhauer J and Michl J. *J. Chem. Soc., Perkin. Trans. 2* 1998: 1101–1118.
22. Fleischhauer J, Höweler U and Michl J. *J. Phys. Chem. A* 2000; **104**: 7762–7775.
23. Fleischhauer J, Höweler U, Spanget-Larsen J, Raabe G and Michl J. *J. Phys. Chem. A* 2004; **108**: 3225–3234.
24. Schleyer PvR, Maerker C, Dransfeld A, Jiao H and van Eikema Hommes NJR. *J. Am. Chem. Soc.* 1996; **118**: 6317–6318.
25. Geuenich D, Hess K, Köhler F and Herges R. *Chem. Rev.* 2005; **105**: 3758–3772.
26. Herges R and Geuenich D. *J. Phys. Chem. A* 2001; **105**: 3214–3220.

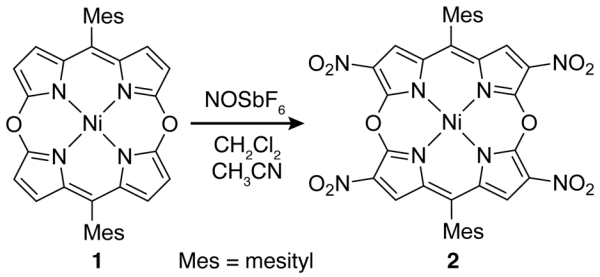

Scheme 1. Synthesis of tetranitro DOP **2** from **1**.

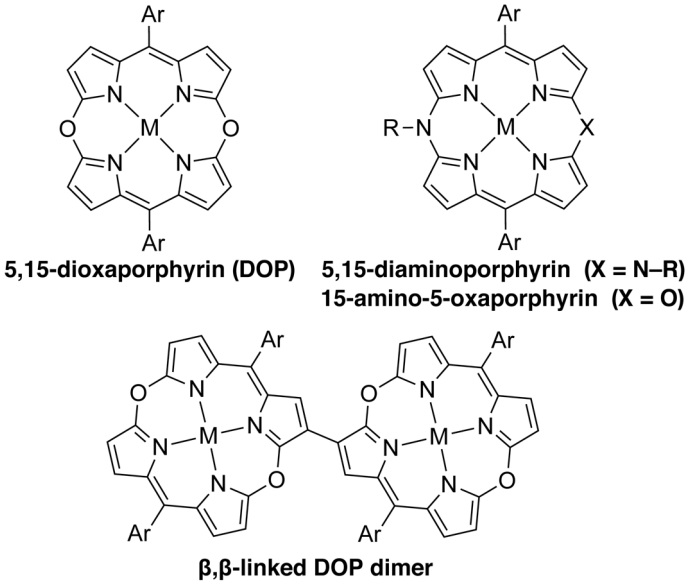

Fig. 1. Structures of 5,15-dioxaporphyrin, 5,15-diaminoporphyrin, 15-amino-5-oxaporphyrin, and β,β-linked DOP dimer.

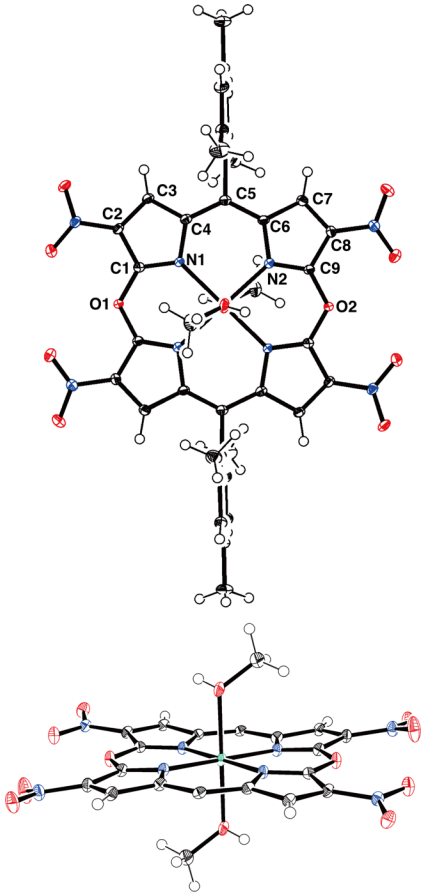

Fig. 2. X-ray single crystal structure of **2**, top view (top) and side view (bottom). The thermal ellipsoids are scaled to the 50% probability level. *meso*-Mesityl-substituents are omitted for clarity in the side view.

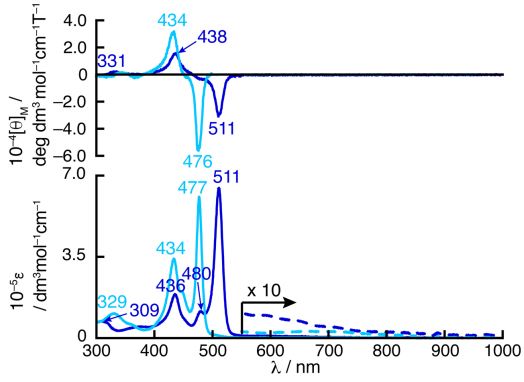

Fig. 3. UV/vis/NIR absorption (bottom) and MCD (top) spectra of **1** (aqua lines) and **2** (blue lines) in $CHCl_3$.

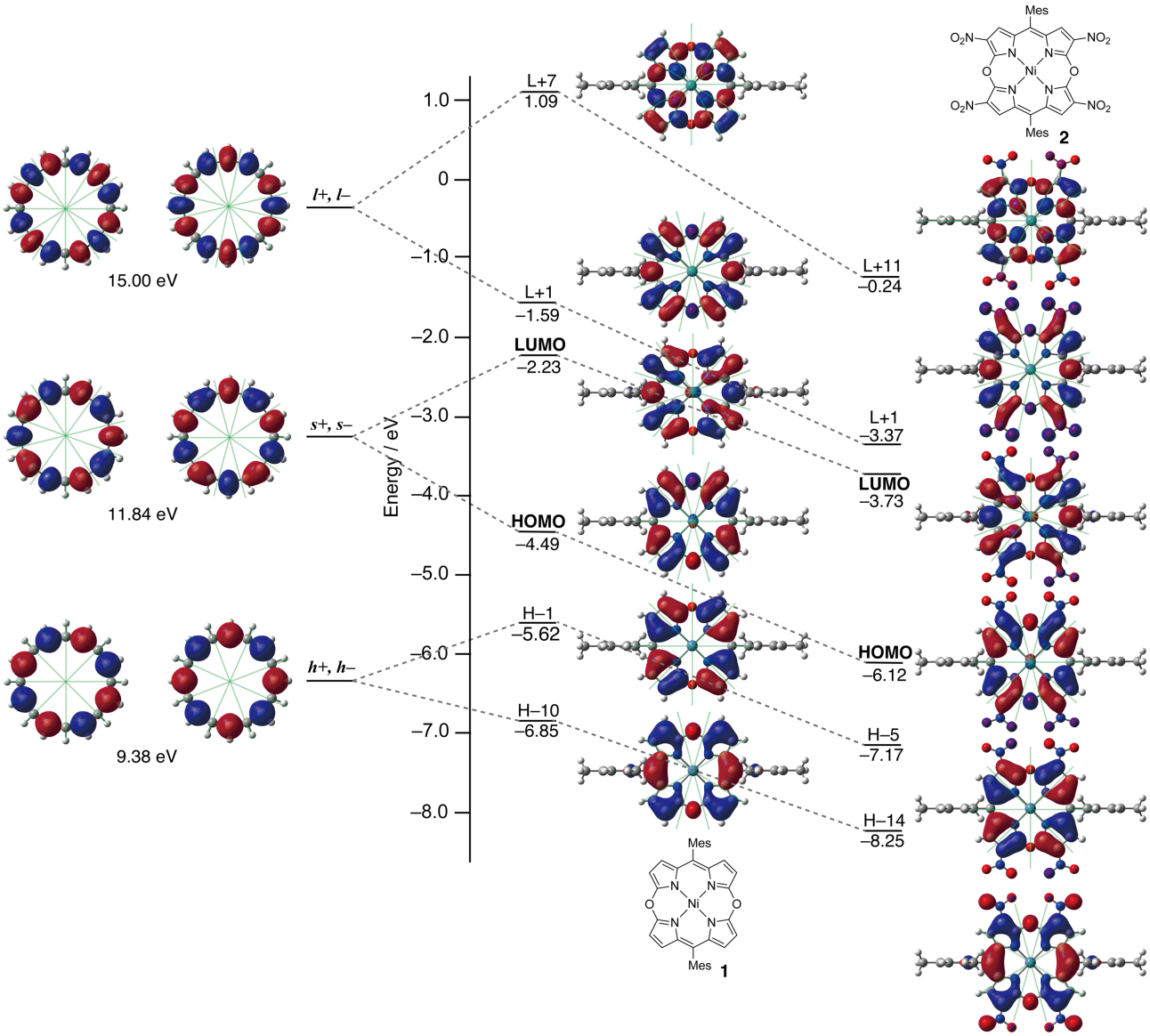

Fig. 4. Frontier molecular orbital diagram of **1** and **2** (B3LYP/ 6-31G(d)) and its 20π-electron [16]annulene perimeter (B3LYP/6-31G(d)). Nodal lines are drawn with pale green lines.

Table 1. Selected transition energies of **2** calculated by the TDDFT method (B3LYP/6-31G(d)).

wavelength [nm]	f [a]	Major contribution (weight%) [b]
669	0.0	H→L (96%), H–8→L+2 (3%)
381	0.81	H–5→L (75%), H→L+1 (15%), H→L+6 (5%)
365	0.14	H→L+3 (98%)
350	0.044	H–7→L+1 (97%)
310	0.049	H–13→L (23%), H→L+6 (69%), H–5→L (4%)
293	0.30	H–20→L (66%), H–14→L (23%), H–23→L (4%)

[a] Oscillator strength. [b] H and L represent HOMO and LUMO, respectively.

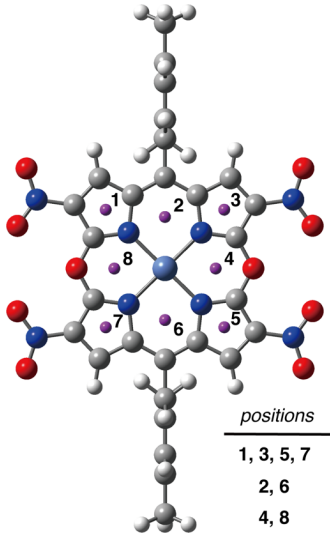

positions	*NICS(1)*
1, 3, 5, 7	–5.3 (–4.3)
2, 6	4.0 (7.7)
4, 8	3.5 (6.7)

Fig. 5. NICS(1) values of **2** at various positions designated in the structure. Values in the parenthesis are NICS(1) values of **1** at the same positions.

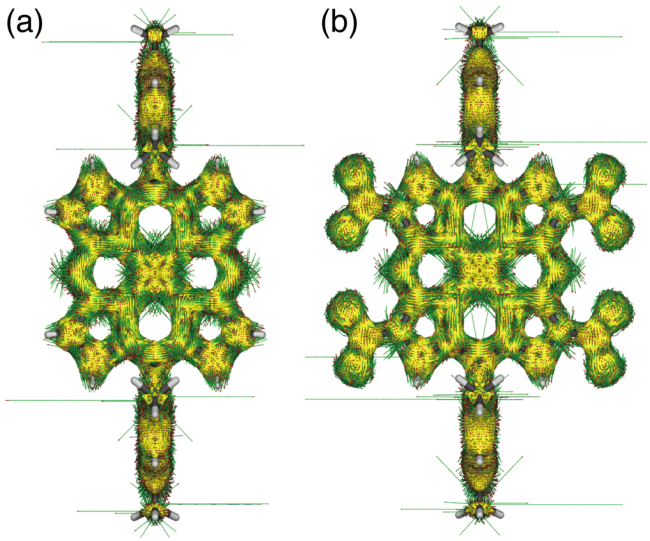

Fig. 6. ACID plots of (a) **1** and (b) **2** (isovalue = 0.05).

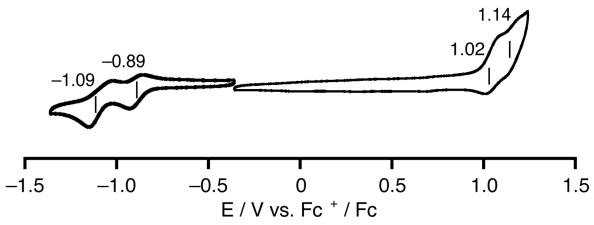

Fig. 7. Cyclic voltammogram of **2** in CH_2Cl_2 containing 0.1 M tetra-*n*-butylammonium hexafluorophosphate at a scan rate of 100 mV s^{-1}.